Journal of Power Sources 189 (2009) 279–287

Contents lists available at ScienceDirect

Journal of Power Sources

journal homepage: www.elsevier.com/locate/jpowsour

Electrochemical studies on $LiCoO_2$ surface coated with $Y_3Al_5O_{12}$ for lithium-ion cells

Jin-Ming Chen[a], Yung-Da Cho[b], Chiao-Ling Hsiao[b], George Ting-Kuo Fey[b,*]

[a] Material Chemical Laboratories, Industrial Technology Research Institute, Hsinchu 310, Taiwan
[b] Department of Chemical and Materials Engineering, National Central University, Chung-Li 320, Taiwan

ARTICLE INFO

Article history:
Received 16 June 2008
Received in revised form 20 August 2008
Accepted 15 September 2008
Available online 24 September 2008

Keywords:
Cathodes
Coated $LiCoO_2$
Cycle stability
Lithium-ion battery
Sol–gel
YAG

ABSTRACT

Synthesized yttrium aluminum garnet (YAG) sol was coated on the surface of the $LiCoO_2$ cathode particles by an in situ sol–gel process, followed by calcination at 923 K for 10 h in air. Based on XRD, TEM, and ESCA data, a compact YAG kernel with an average thickness of ~20 nm was formed on the surface of the core $LiCoO_2$ particles, which ranged from ~90 to 120 nm in size. The charge–discharge cycling studies for the coated materials suggest that 0.3 wt.% YAG-coated $LiCoO_2$ heated at 923 K for 10 h in air, delivered a discharge capacity of 167 mAh g^{-1} and a cycle stability of about 164 cycles with a fading rate of 0.2 mAh $cycle^{-1}$ at a 0.2*C*-rate between 2.75 and 4.40 V *vs.* Li/Li^+. The differential capacity plots revealed that impedance growth was slower for YAG surface treated $LiCoO_2$, when cells were charged at 4.40 V. DSC results exemplified that the exothermic peak at ~468 K corresponded to the release of much less oxygen and greater thermal-stability.

1. Introduction

Lithiated transition metal oxides, $LiCoO_2$, $LiNiO_2$, $LiMn_2O_4$, are most commonly used in lithium-ion batteries as cathode materials for various applications [1–3]. Layered $LiCoO_2$ is the most stable cathode material because of its excellent reversibility, high energy density, ease of preparation, low weight and small volume [1–5]. However, it has a specific capacity of 274 mAh g^{-1}. During the (de)lithiation process from 2.75 to 4.20 V vs. Li/Li^+, by experimentation, only 0.5 Li^+ per molecule of $LiCoO_2$ can be extractable and thereby possesses 137 mAh g^{-1} capacity [6]. Hence, in order to obtain a higher capacity, the cathode materials have to be delithiated beyond 4.20 V. As a result, cathode materials charged at higher voltages, suffer from significantly lower cycle stability due to the structural instability caused by easy dissolution of Co^{4+} into the acidic electrolyte medium, as well as a large number of side reactions on the surface of the cathode particles. All these factors cause faster impedance growth on the surface of the particles and rapid capacity fades [7,8].

Therefore, attempts have been made to improve the electrochemical performance and cycle stability by doping non-transition and transition metal ions into the $LiCoO_2$ structure by partial substitution of cobalt, but the methods resulted in only substandard capacity and cycle stability [9,10]. The inferior results directed the researchers to an alternative approach that involves modifying the surface of the cathode material by coating it with electrochemically inactive metal oxides. The surface coated cathode materials can deliver stable capacities when cycled even beyond 4.50 V and enhanced electrochemical performance and cycle stability upon surface treatment. A wide range of research was carried out on both layered and spinel oxides to improve cycle stability by the surface coating technique. The surface coated with ZrO_2 [7,8,11,12], Al_2O_3 [7,11–17], TiO_2 [11,12,18], SiO_2 [8,19], Co_3O_4 [20] and La_2O_3 [21], demonstrated enhanced discharge capacity and cycling behavior. The materials used for surface coating play a significant role between the core materials and the acidic electrolyte by protecting the highly active core material (3d metal ion) from diffusion and dissolution into the acidic electrolyte, thereby preventing many side reactions that would lead to faster impedance growth.

The surface coating materials and techniques [7,8,11–21] employed for coating play a critical role in the formation of a uniform and well-adhered coating on the core material surface with low temperature syntheses. In general, ceramic materials are suitable candidates due to their high thermo-mechanical stability, resistance to both oxidizing and reducing atmospheres at high temperatures, and resistance to attack by moisture and chemical reactions [22–24]. Of all the ceramic materials currently being investigated, yttrium based ceramic powders are promising

* Corresponding author. Tel.: +886 3 425 7325; fax: +886 3 425 7325.
E-mail address: gfey@cc.ncu.edu.tw (G.T.-K. Fey).

0378-7753/$ – see front matter © 2008 Elsevier B.V. All rights reserved.
doi:10.1016/j.jpowsour.2008.09.049

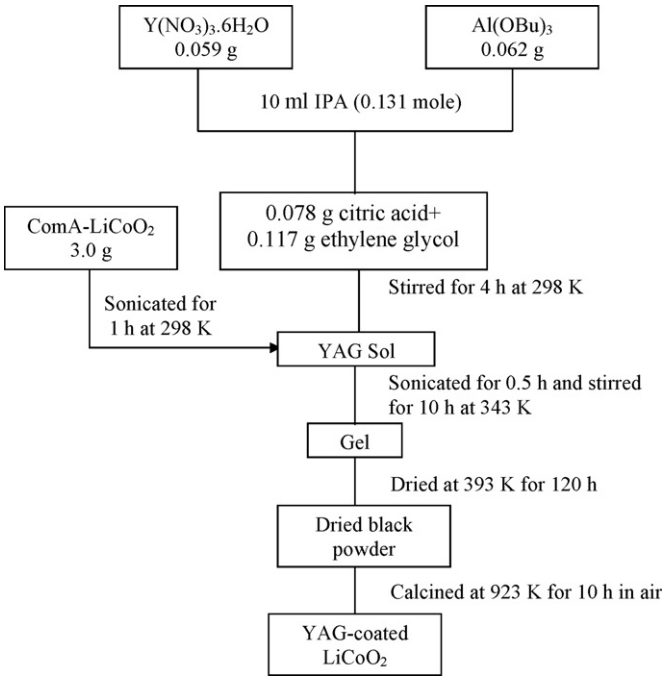

Fig. 1. Schematic for the YAG-coated $LiCoO_2$ cathode material prepared by an in situ sol–gel method.

materials for optical, electronic and structural applications. The composition $3Y_2O_3{:}5Al_2O_3$, commonly called yttrium aluminum garnet (YAG), adopted the cubic garnet structure and was vital to the fabrication of solid-state lasers widely used in luminescence systems and high-temperature chemically stable and extremely high creep resistance material. The significance of YAG ceramic powder focused our attention to preparing various wt.% YAG sol coatings on the $LiCoO_2$ cathode materials by an in situ sol–gel process and studying its optimum composition, calcination temperature and time based on its electrochemical cell performance and thermal stability when charged at 4.40 V.

2. Experimental

2.1. Synthesis of YAG coating material by sol–gel process

Yttrium aluminum garnet (YAG, $Y_3Al_5O_{12}$) ceramic powder was synthesized through an alkoxide based sol–gel process [24]. Analytical grade chemicals used in the preparation process were aluminum tert-butoxide ($Al(OC_4H_9)_4$) (Aldrich), yttrium nitrate hexahydrate ($Y(NO_3)_3{\cdot}6H_2O$) (Aldrich), isopropyl alcohol (IPA), citric acid and ethylene glycol. Initially both $Al(OC_4H_9)_4$ and ($Y(NO_3)_3{\cdot}6H_2O$) solution were prepared separately in IPA and mixed together to form the yttrium alumina sol precursor, in addition to citric acid and ethylene glycol which were added as complexing agents. The sol was allowed to set into a gel at 343 K, maintained in an oven, and the gel later aged at 393 K for 5 days. The dried gel was heated at 723, 823 and 923 K for 5 h at a heating ramp of 2 K min^{-1} to yield brown crystalline $Y_3Al_5O_{12}$ ceramic powders.

2.2. In situ sol–gel synthesis YAG-coated $LiCoO_2$

YAG ceramic sol was synthesized as described in Section 2.1, and Fig. 1 shows the complete in situ sol–gel procedure for the synthesis of YAG-coated $LiCoO_2$ cathode material. The calculated amount of $LiCoO_2$ cathode powder was dispersed in IPA and added to the in situ synthesized YAG sol precursor by a 0.5 h sonication followed by continuous stirring for 10 h at 343 K. After the removal of excess IPA, a thick black gel was formed. The obtained gel was dried in an oven at 393 K for 120 h to form a dry black powder, which was heated at 923 K for 10 h in air at a heating ramp of 2 K min^{-1} to form a thin layer of YAG coating on $LiCoO_2$ with the weight ratios of 0.1:99.9, 0.3:99.7, 0.7:99.3, 1.0:99.0 and 1.5:98.5.

Structural and phase analyses were carried out using a powder X-ray diffractometer (XRD), Siemens D-5000, Mac Science MXP18, equipped with a nickel-filtered Cu-K_α radiation source (λ = 1.5405 Å). The diffraction patterns were recorded between scattering angles of 15° and 80° in steps of 0.05°. The surface morphology of the coated materials was studied using a scanning electron microscope (SEM), Hitachi model S-3500 V. The sol–gel synthesized YAG particle size and the coating layer morphology of the coated particle was examined by a JEOL JEM-200FXII transmission electron microscope (TEM) equipped with a LaB_6 gun. The sample for TEM study was prepared by dispersing the powder in ethanol, placing a drop of the clear solution on a carbon-coated copper grid, and subsequent drying. The depth profiles of yttrium, aluminum, cobalt and oxygen were recorded by an electron spectroscopy for chemical analysis (ESCA) instrument (VG Scientific ESCALAB 250) with monochromatic Mg-K_α radiation 1253.6 eV.

The cathodes for electrochemical studies were prepared by a doctor-blade coating method with a slurry of 85 wt.% coated active material, 10 wt.% conductive carbon black and 5 wt.% poly(vinylidene fluoride) as a binder, in N-methyl-2-pyrrolidone (NMP), as the solvent for the mixture, which was then applied onto an etched aluminum foil current collector and dried at 393 K for 12 h in an oven. The coated cathode foil was then smoothed by pressing it through stainless-steel twin rollers and cut into circular discs 13 mm in diameter.

The electrochemical performance of the above discs were evaluated with coin type cells of the 2032 configuration and were assembled in an argon-filled VAC MO40-1 glove box in which the oxygen and water contents were maintained below 2 ppm. Lithium metal (Foote Mineral) was used as the anode and a 1 M solution $LiPF_6$ in ethylene carbonate:diethyl carbonate EC:DEC (1:1, v/v) (Tomiyama Chemicals) was used as the electrolyte with a Celgard membrane as the separator. The cells charge–discharge cycles were preformed at a 0.2*C*-rate between 2.75 and 4.40 V at 293 K, in a multi-channel battery tester (Maccor 4000).

Thermal stability analysis was carried out on a PerkinElmer DSC 7 differential scanning calorimetry (DSC) for the pristine and the YAG-coated $LiCoO_2$ cathode materials. The measurements were performed in a nitrogen atmosphere between 323 and 623 K, at a heating rate of 3 K min^{-1}. The samples for the DSC investigations were prepared as follows. The coin cells were first galvanostatically charged to 4.40 V at a 0.2*C*-rate and then potentiostated at 4.40 V for 20 h. The coin cells were dismantled in an argon-filled glove box and the charged cathode was carefully removed. The cathode was then washed with DEC. The excess electrolyte was wiped off and dried. The cathode material was gently scraped from the alumina current collector, loaded on to an aluminum pan, sealed air tight, and transferred to the DSC instrument for measurement.

3. Results and discussion

3.1. X-ray diffraction

Fig. 2a–d shows the XRD patterns of sol–gel prepared YAG ceramic dried gel heated at 723, 823, 923 K and JCPDS #88-2047 of YAG, respectively. From Fig. 2a and b, the as-prepared dried gel heated at 723 and 823 K remained a crystalline embedded

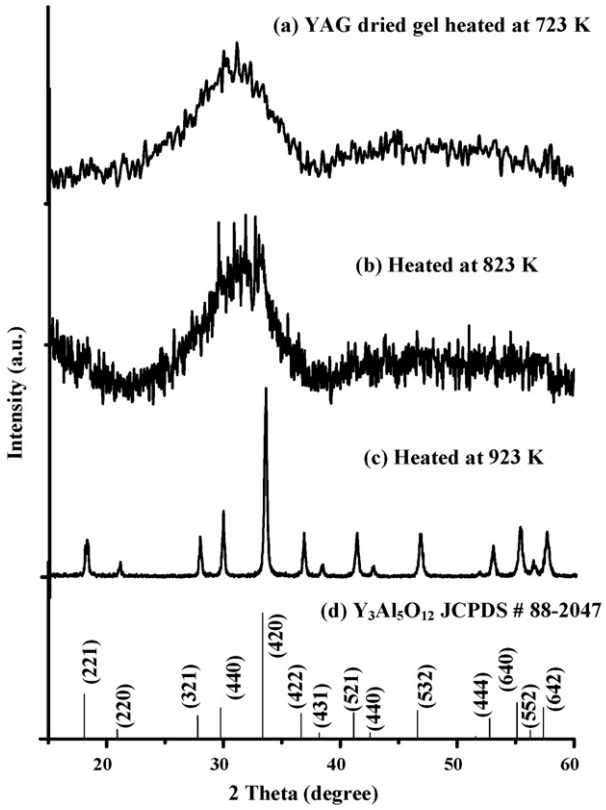

Fig. 2. X-ray diffraction patterns of the sol–gel synthesized YAG heated at (a) 723 K, (b) 823 K, (c) 923 K and (d) JCPDS #88-2047 of YAG.

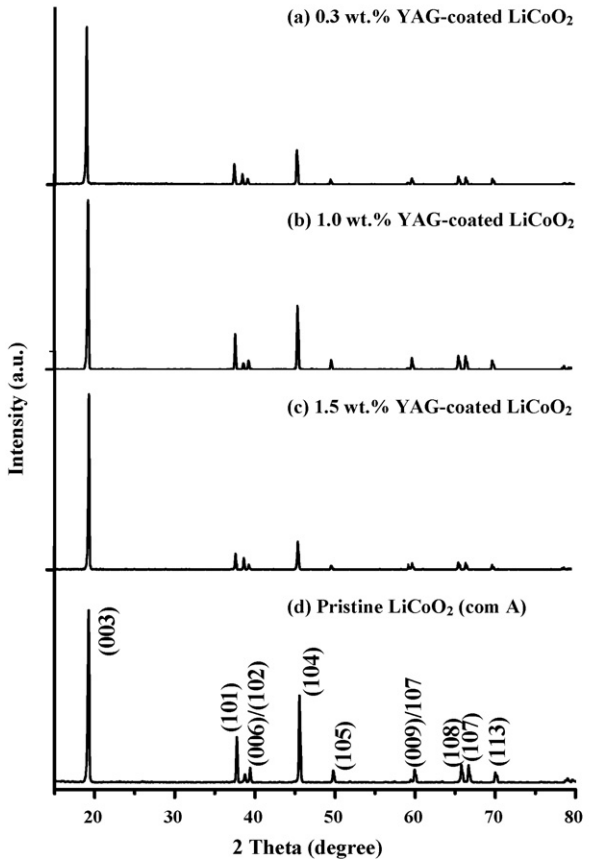

Fig. 3. X-ray diffraction patterns of (a) 0.3, (b) 1.0, (c) 1.5 wt.% of YAG-coated and (d) pristine $LiCoO_2$.

amorphous compound and heat treatment above 823 K resulted in complete crystallinity. In Fig. 2c, it is clearly noted that a comprehensive crystalline single-phase material was obtained, when calcined at 923 K for 5 h in air. The pure phase of the synthesized YAG material could be indexed to the JCPDS #88-2047 pattern [25] as shown in Fig. 2d, which belongs to the cubic crystalline structure.

Fig. 3a–d shows the XRD patterns of in situ sol–gel prepared 0.3, 1.0, 1.5 wt.% YAG-coated $LiCoO_2$ heated at 923 K for 10 h in air and pristine $LiCoO_2$, respectively. The diffraction patterns of all the coated materials conform to a single-phase hexagonal structure of α-$NaFeO_2$ type with space group $R\bar{3}m$ symmetry of the core material compared to the pristine $LiCoO_2$ cathode material. The absence of secondary phase diffraction patterns corresponding to YAG may be due to very low concentrations of YAG, but the presence of a YAG coating layer was confirmed by ESCA analysis provided in a later section. Table 1 presents the lattice parameters *a* and *c* and *R*-factor values of the pristine $LiCoO_2$ and the YAG-coated materials, which suggest that the coated particles show basic small changes in the lattice parameters, indicating that YAG does not form a solid solution by interacting with core material during the calcination process at 923 K for 10 h. Dahn et al. [26,27], reported that the *R*-factor is an indicator of hexagonal ordering and a lower *R*-factor level identifies better hexagonal ordering and electrochemical performance. From Table 1, it is noticeable that the *R*-factor levels were lower for the coated materials than the pristine cathode material and that indicates better hexagonal ordering and matches well with the enhanced electrochemical performance in illustrated in a later section.

Table 1
XRD data on the pristine $LiCoO_2$ and YAG-coated $LiCoO_2$ cathode materials.

YAG coating level	*a* (Å)	*c* (Å)	*c*/*a*	*R*-factor
Pristine $LiCoO_2$	2.810	13.938	4.960	0.772
0.1 wt.%	2.802	13.757	4.909	0.625
0.3 wt.%	2.814	14.030	4.986	0.421
0.7 wt.%	2.800	13.677	4.885	0.446
1.0 wt.%	2.805	13.828	4.929	0.472
1.5 wt.%	2.803	13.772	4.913	0.673

The X-ray diffractograms of 0.3 wt. % YAG-coated $LiCoO_2$ synthesized by calcination at 923 K for different durations are presented in Fig. 4. The diffraction patterns of all the materials conform to a single-phase hexagonal structure with space group $R\bar{3}m$ symmetry of the core material. However, the diffractograms tended to become sharper as the calcination period was increased, indicating that the crystallinity of the products improved with longer calcination time. The 2θ values in the XRD patterns of the YAG-coated particles did not change, which indicated that YAG did not form a solid solution by interacting with the core material during the longer calcinations time.

3.2. Morphology

3.2.1. SEM

Fig. 5a and b shows the SEM micrographs of pristine $LiCoO_2$ and 0.3 wt.% YAG-coated $LiCoO_2$, respectively. From Fig. 5a and b, it is clear that the surface of the cathode particles changed after surface treatment of the particles with YAG. The coated particles were brighter on the surface compared to pristine $LiCoO_2$ and this is associated with the accumulation of charge on the non-conducting YAG coating material as the electron beam impinges on it. Thus, it is evi-

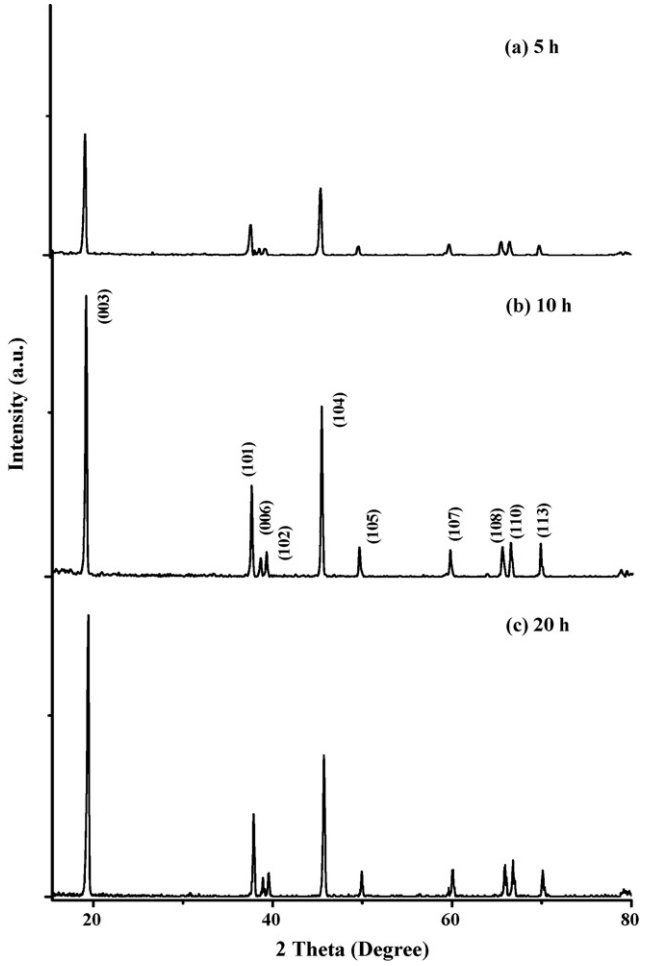

Fig. 4. X-ray diffraction patterns of 0.3 wt.% YAG-coated $LiCoO_2$ heated for different time periods: (a) 5 h, (b) 10 h, (c) 20 h.

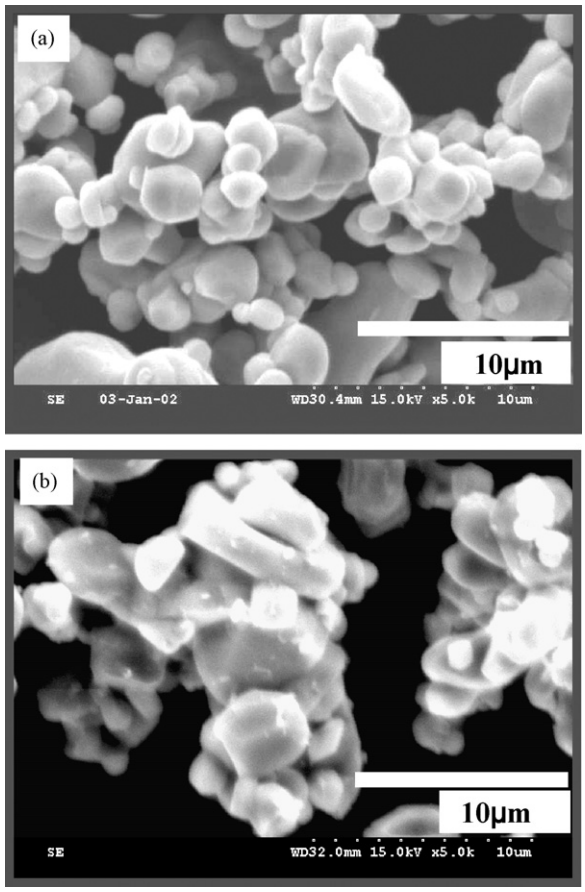

Fig. 5. SEM micrographs of (a) pristine and (b) 0.3 wt.% of YAG-coated $LiCoO_2$.

dent from the SEM images that the surface of the cathode material remained modified with YAG coating.

3.2.2. TEM

Fig. 6a–d shows the TEM images of YAG ceramic powder prepared by a sol–gel process and 0.1, 0.3, 1.5 wt.% YAG-coated $LiCoO_2$, respectively. In Fig. 6a, the sol–gel prepared YAG particle was formed of uniform nanosized particles in a range of 90–120 nm. The micrograph in Fig. 6b combined with the cycle results from Fig. 9 clearly illustrates that a concentration of 0.1 wt.% YAG coating level is too low to form a sufficient compact coating on the core material and to protect the surface reaction. At the 0.3 wt.% YAG concentration, a translucent layer of YAG particles was formed in a compact well-adhered thin film over the $LiCoO_2$ surfaces that had an average thickness of about ~20 nm, as shown in Fig. 6c. This level of coating was shown to be sufficient based on the good cycle behavior in Fig. 8. However, as the YAG concentration further increased, cycle stability of the YAG-coated material decreased. The 2.0 wt.% YAG-coated $LiCoO_2$ particle (Fig. 6d) showed a remarkable thick and non-uniform coating on the surface of the $LiCoO_2$ particles.

3.3. ESCA

Fig. 7 shows the spatial distribution of yttrium and aluminum atomic concentrations in YAG-coated $LiCoO_2$ with a depth profile of the particle up to 100 nm. In Fig. 7, the concentration of yttrium and aluminum were low, typically less than the one atomic percent at the surface level and beyond that there was a decrease in the concentrations of the ions with the depth of the particle. The ESCA results revealed that the coating is formed of a thin YAG layer on the surface of the core material.

3.4. Electrochemical properties

3.4.1. Cycling behavior at various calcination temperatures

Fig. 8 shows the discharge curves between 2.75 and 4.4 V for pristine $LiCoO_2$ and 1.0 wt.% YAG-coated $LiCoO_2$ calcined at 723, 823, 923 and 1023 K for 10 h in air. The effect of calcination temperatures for the YAG-coated sample was compared to pristine $LiCoO_2$ with a preset cut-off value of 80% capacity retention calculated based on the first-cycle discharge capacity of the respective material and optimized the calcination temperature. The charge–discharge plots in Fig. 8 shows the enhanced cycle stability upon coating with YAG on the surface of the pristine $LiCoO_2$ particles. Compared to the cut-off capacity retention for pristine $LiCoO_2$, it delivered an initial capacity 162 mAh g^{-1} and could sustain just 24 cycles. From Fig. 8, it is apparent that the number of cycles sustained by 1.0 wt.% YAG-coated $LiCoO_2$ sample heated at 923 K was 153 cycles with an initial capacity 166 mAh g^{-1} compared to the samples heated at 723, 823 and 1023 K which delivered 119, 118 and 121 cycles, respectively. Therefore, the electrochemical performance for the samples calcined at different temperatures demonstrated that the 923 K heated sample exhibited better cycling behavior. Hence, the optimal calcination temperature was 923 K, based on the possible formation of a well-adhered coating layer with core particles at that temperature.

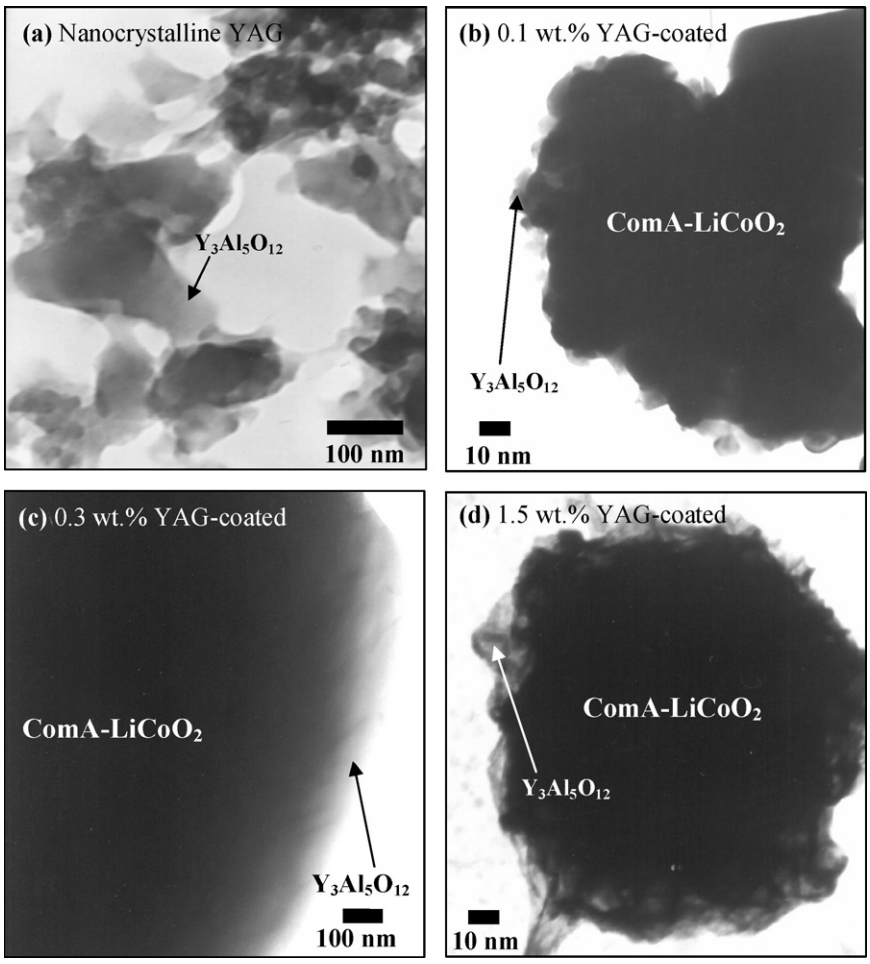

Fig. 6. TEM images of (a) nanocrystalline YAG, (b) 0.1 wt.%, (c) 0.3 wt.%, (d) 1.5 wt.% YAG-coated $LiCoO_2$ particle synthesized by an in situ sol–gel method.

3.4.2. Cycling behavior of various wt.% YAG-coated $LiCoO_2$

Fig. 9 shows the discharge curves for the pristine $LiCoO_2$, 0.1, 0.3, 0.7, 1.0 and 1.5 wt.% YAG-coated $LiCoO_2$ samples, calcined at 923 K for 10 h in air. The effect of various wt.% of YAG coating on the cycle stability and performance of the cells were demonstrated based on a preset cut-off value of 80% capacity retention and calculated with the first-cycle discharge capacity of the respective material. It can be seen from Fig. 9 that the charge–discharge performance for the YAG surface coated samples was enhanced compared to the cycle stability offered by the pristine $LiCoO_2$ cathode materials. Based on the cut-off capacity retention, the pristine $LiCoO_2$ could sustain just 24 cycles and delivered an initial capacity 162 mAh g^{-1}. The number of cycles sustained by 0.1, 0.3, 0.7, 1.0 and 1.5 wt.% YAG-coated samples were 94, 164, 145, 154 and 130 cycles, respectively. The cycle performance results revealed that the 0.3 wt.% YAG-coated $LiCoO_2$ sample could sustain 164 cycles compared to the other com-

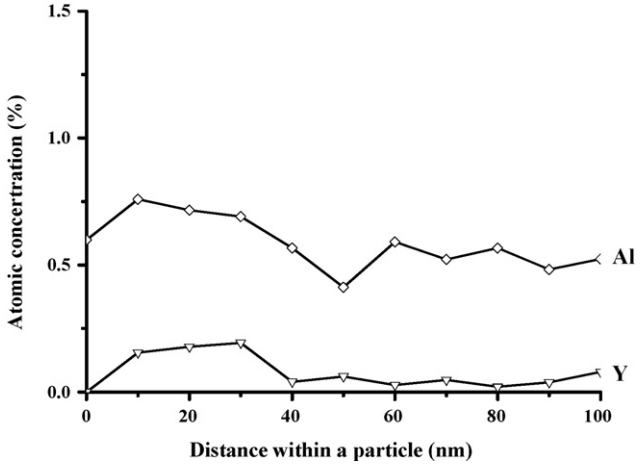

Fig. 7. Depth profile of a 0.3 wt.% YAG-coated $LiCoO_2$ particle.

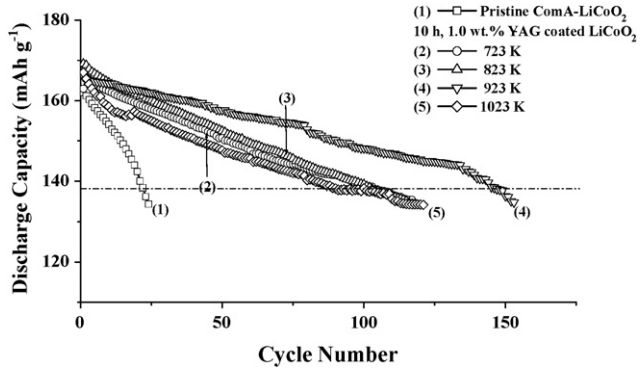

Fig. 8. Discharge curves of pristine and different heat treatment temperature for 1.0 wt.% YAG-coated $LiCoO_2$ synthesized by an in situ sol–gel method. Charge–discharge: 4.40–2.75 V; 0.2C-rate.

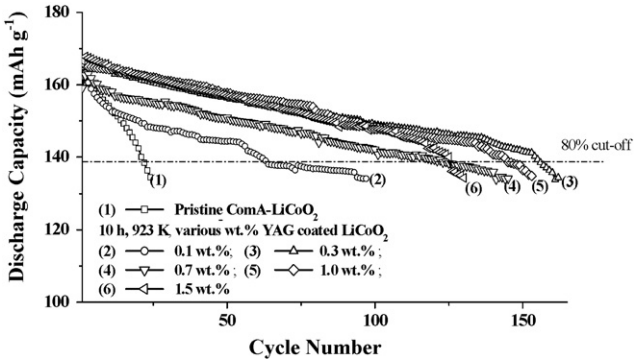

Fig. 9. Discharge curves of pristine and various wt.% YAG-coated $LiCoO_2$ synthesized by an in situ sol–gel method. Charge–discharge: 4.40–2.75 V; 0.2*C*-rate.

positions and the pristine $LiCoO_2$ cathode. The TEM results (Fig. 6b) clearly illustrated that a very low concentration of 0.1 wt.% could not protect the surface reaction from occurring on the particle, because there was an insufficient compact coating on the core material. Even though higher coating levels, such as 0.7, 1.0 and 1.5 wt.%, sustained better cycle stability than pristine $LiCoO_2$, compared to a 0.3 wt.%-coated sample, they showed less stability. The presence of excess coating material between the particles can hinder particle–particle electronic conductivity and adversely affect the coulombic efficiency. Therefore, it is noteworthy that the 0.3 wt.% YAG coating level is optimal for this material to form a compact coating with a lesser amount, which is advantageous from a practical point of view. The YAG coating material could protect the core material from the acidic electrolyte when the cells were charged to 4.40 V and hinder the strongly oxidized Co^{4+} ions from participating in a side reaction with the acidic electrolyte so that it reduces the formation of a thick inactive layer on the surface of the cathode particle, which would lead to declined capacity fade [28]. Therefore, the optimum level of 0.3 wt.% YAG could sustain good cycle stability and better cell performance.

3.4.3. Cycling behavior for calcination time

Fig. 10 compares the cycle stability of 0.3 wt.% YAG-coated $LiCoO_2$ calcined at 923 K for different periods: 5, 10, 20 h. It can be seen that while the 5 and 20 h calcined samples sustained 138 and 14 cycles and first discharge capacities were 171 and 165 mAh g^{-1}, respectively, the 10 h calcined sample sustained 164 cycles before reaching the 80% charge retention cut-off value. The inferior performance of the 5 h calcined material reflects the poor crystallinity of the product, as noted from the XRD patterns (Fig. 4). Furthermore, the calcination time was too short to form a complete compact and well-adhered coating surface on the core material that could lengthen cycle-life. On the other hand, a long calcination time at 923 K, such as 20 h, resulted in severe capacity fade, because the lithium is prone to evaporate at high temperature during extended heating times. In this study, it is clear that the 0.3 wt.% YAG-coated sample heated at 923 K for 10 h had the best cell performance and this is attributed to the formation of a well-adhered coating on the surface, as shown in Fig. 6c.

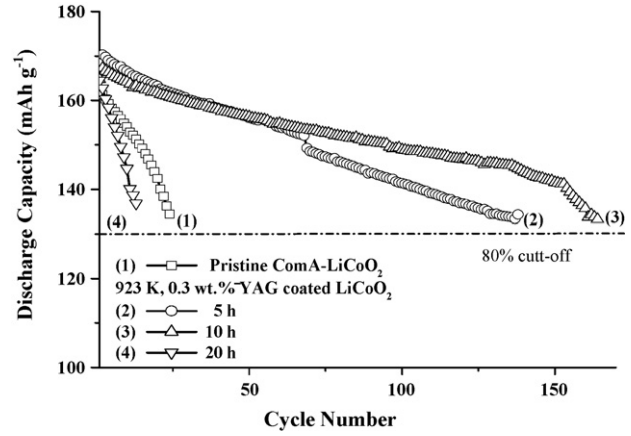

Fig. 10. Discharge curves of 0.3 wt.% YAG-coated $LiCoO_2$ synthesized by an in situ sol–gel method and heated for different time periods. Charge–discharge: 4.40–2.75 V; 0.2*C*-rate.

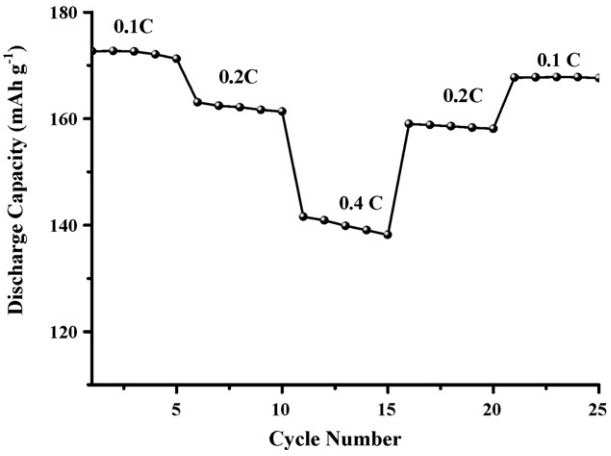

Fig. 11. Discharge curves of 0.3 wt.% YAG-coated $LiCoO_2$ synthesized by an in situ sol–gel method. Charge–discharge: 4.40–2.75 V at 0.1, 0.2 and 0.4*C*-rates.

3.4.4. Cycling behavior of coated samples at different C-rates

Fig. 11 shows the consequence of YAG coating on the rate capability with cycle performance for the cell cycled between 2.75 and 4.40 V at different *C*-rates such as 0.1, 0.2 and 0.4*C*. In Fig. 11, a relatively high discharge capacity of 173 mAh g^{-1} was achieved at 0.1*C*, but at 0.2*C*, the discharge capacity suddenly decreased to 163 mAh g^{-1}, with small capacity fading during cycling and low irreversible capacity loss. Further cycling at 0.4*C*, caused the cell to exhibit an even lower discharge capacity of 141 mAh g^{-1}. There was a large fall in the discharge capacity with an increase in *C*-rate because lithium ion diffusion and electronic conduction were limited. However, when the *C*-rates were applied in declining order, 0.4, 0.2 and 0.1*C*, the cell was able to repossess its higher capacity at lower *C*-rates. YAG itself is ceramic, dense, compact, and not electronically conductive. The YAG coating layer provides only a protective compact layer, but does not block the channels for Li-ions diffusion. However, the function of these channels gradually decayed as the charge–discharge process proceeded. The coating layer can hinder the strongly oxidized Co^{4+} ions from participating in a side reaction with the acidic electrolyte, and form a passivation layer on the surface of the electrode that inhibits lithium ion movement. Accordingly, a YAG-coated $LiCoO_2$ cathode has limited rate capability.

Fig. 12a shows the dQ/dV *vs.* voltage plots of pristine $LiCoO_2$ cathode between 2.75 and 4.40 V for 5, 10, 20 and 24 cycles at 298 K. Fig. 12b shows the dQ/dV *vs.* voltage of 0.3 wt.% YAG-coated $LiCoO_2$ for 5, 10, 50, 105 and 164 cycles. From Fig. 12a, it is observed that the charge–discharge peaks centered at 3.97 and 3.83 V, respectively, are narrow and sharp corresponding to (de)lithiation process. However, after 24 continuous cycles, the pristine $LiCoO_2$ showed that the transition peaks became broader and shifted to 4.05 and 3.76 V. In Fig. 12b, the peaks corresponding to the phase transition during charge–discharge process were centered at 3.95 and 3.85 V, respec-

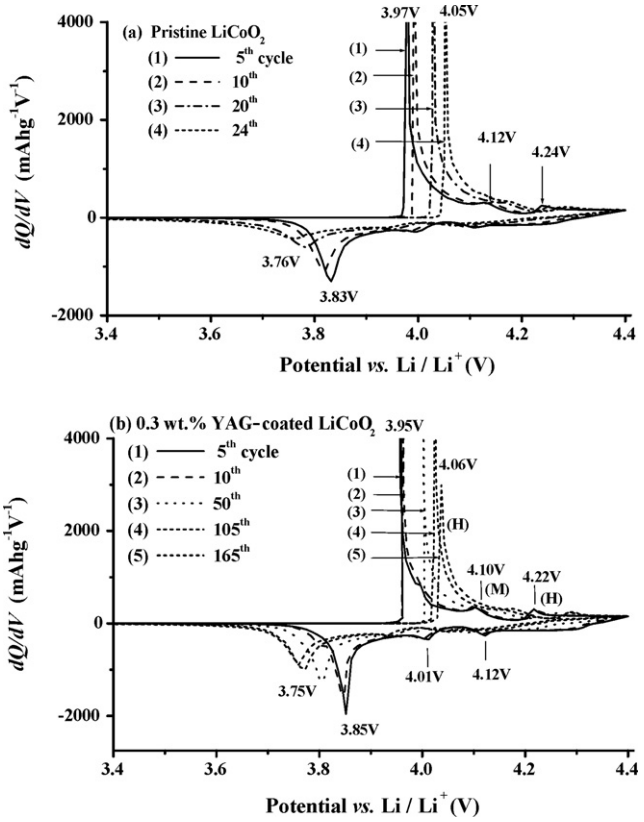

Fig. 12. The d*Q*/d*V* vs. voltage curves of (a) $LiCoO_2$ pristine and (b) 0.3 wt.% YAG-coated $LiCoO_2$ synthesized by an in situ sol–gel method. Charge–discharge at 4.40–3.40 V; 0.2*C*-rate.

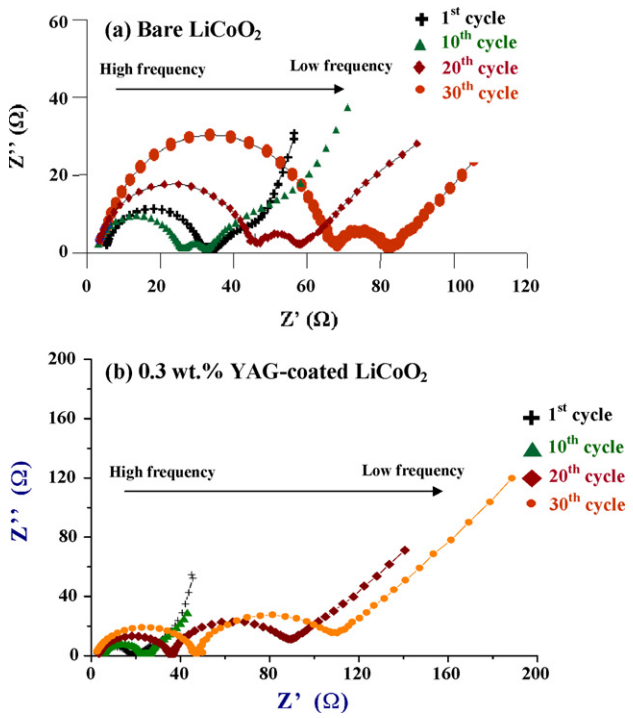

Fig. 13. Nyquist plots of (a) bare, and (b) 0.3 wt.% YAG-coated $LiCoO_2$ as a function of cycle number.

tively, were narrow and sharp, and after continuous 164 cycling, the peaks shifted to 4.06 and 3.75 V. From the results, it is clear that the pristine sample exhibited a large shift between the reduction peaks of ~0.07 V for only 24 cycles, but the coated samples showed the reduction peaks shifted less at ~0.10 V for 164 cycles [7,8]. Moreover, it is obvious from the differential plots that the phase suppression was not involved during the cycling process for the coated and uncoated samples. Thus, it is evident that the large capacity fade during 24 cycles for the pristine sample was the result of faster impedance growth on the surface of the pristine cathode occurred during the charge–discharge process.

The better cycle stability possessed by 0.3 wt.% YAG-coated $LiCoO_2$ could be attributed to slower impedance growth on the surface of the materials due to the presence of a highly stable inert ceramic surface layer of YAG, which prevented direct contact between the core materials and the acidic electrolyte and prevented the loss of 3d metal ions into the electrolyte. In general, impedance growth must be caused by some side reactions at the surface of active pristine $LiCoO_2$. Aurbach et al. [29] reported that $LiCoO_2$ cathodes undergo a gradual degradation upon cycling and the causes for the major capacity fade mechanism involved the formation of thickened surface films on the surface of the cathode materials. These results were supported by Edstrom et al. [30] from reported XPS data, where the cathode material surface was formed of organic species and their reactions with the lithium-salt anion were more dependent on the electrode material type. It is particularly vital to decrease the impact of the PF_6 anion and its related contaminants (HF and PF_5) on electrode surface chemistry through the implementation of more stable salts. YAG, being a stable and inert ceramic material to the chemical reaction and temperature helped improve cycle stability by primarily protecting the cathode surface from the growth of a thick impedance film, which is attributed to the surface chemistry of $LiCoO_2$ and the reactivity of the acidic electrolyte.

3.5. Electrochemical impedance

The Electrical impedance spectroscopy (EIS) response of pristine $LiCoO_2$ and 0.3 wt.% YAG-coated $LiCoO_2$ cathodes in non-aqueous electrolytes reveals the processes such as the transport of lithium ions in the electrolyte, charge-transfer across the electrode/electrolyte interface, and adsorption of absorbed lithium ions into the solid oxide matrix [31,32]. Fig. 13a and b compares the EIS profiles of pristine $LiCoO_2$ and 0.3 wt.% YAG-coated $LiCoO_2$ cathodes before and after cycling. In Fig. 13a and b, the high frequency semicircle represents the impedance due to a surface film on the oxide electrode, while the low frequency semicircle is related to a slow charge transfer process at the interface, as well as a capacitance at the oxide interface. The Warburg tail implies that the electrode processes under this condition are controlled by diffusion. The impedance spectra were analyzed by Z-view software and the data fitted to the equivalent circuit shown in Fig. 14. Here, R_e is the electrolyte resistance, R_p the particle-to-particle resistance,

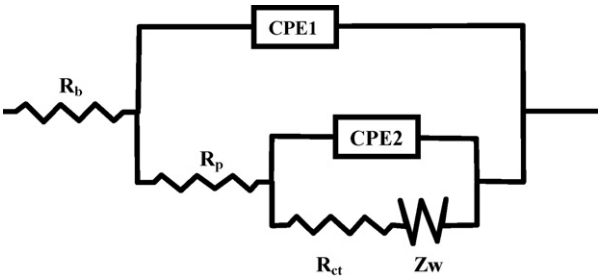

Fig. 14. Equivalent circuit used for fitting impedance data.

Table 2
Variation in the particle-to-particle resistance as a function of cycle number (a) bare, and (b) 0.3 wt.% YAG-coated $LiCoO_2$.

Coating precursor	Cycle number	R_e (Ω)	R_p (Ω)	R_{ct} (Ω)
Bare $LiCoO_2$	1	5.56	15.74	5.14
	10	2.41	22.46	7.50
	20	2.63	40.85	14.40
	30	3.25	75.52	30.41
$Y_3Al_5O_{12}$	1	2.27	15.09	3.6
	10	2.23	17.35	3.15
	20	3.51	33.08	49.65
	30	3.82	45.62	55.37

R_{ct} the charge-transfer resistance, W the Warburg impedance, and CPE1 and CPE2 are constant phase elements.

The solution resistance, R_e, underwent very small changes upon cycling from 5.56 to 3.25 Ω in the case of pristine and 2.27–3.82 Ω for the YAG-coated material (as shown in Table 2). The slight changes in solution resistance were attributed to the complex chemistry of lithium in electrolyte solutions that caused slight changes in the content of the conducting species in the solution [33]. However, the size of the semicircle was larger for the pristine material than for the coated material. An evaluation of the changes in resistance of the pristine and coated cathodes as a function of cycle number showed that the resistance of the surface film on the bare cathode particles increased faster from 25 to 68 Ω for 30 cycles. In contrast, the resistance of the coated cathode material remained at 45 Ω even after 30 cycles. The results revealed that pristine $LiCoO_2$ had a compact surface film of polycarbonates, alkyl carbonates and LiF [34,35,29]. The composition of this film changed with the incorporation of oxide reaction products into the electrolyte constituents. Thus, during repeated cycling, the inactive surface film was transformed into a thick dense layer with the incorporation of other products, raising its resistance and resulting in an inactive cathode material. On the other hand, the YAG coated cathode seemed to make the cathode less prone to changes, because YAG behaved like an amphoteric and scavenged the acidic HF species from the $LiPF_6$ liquid electrolyte. According to Aurbach et al. [36], although $LiCoO_2$ cathodes undergo a gradual degradation upon cycling, the major capacity fade mechanism involves the formation and thickening of surface films. Therefore, we conclude that YAG significantly prevents the formation of surface film as cycling proceeds and maintains the capacity of the cell over a longer cycle life.

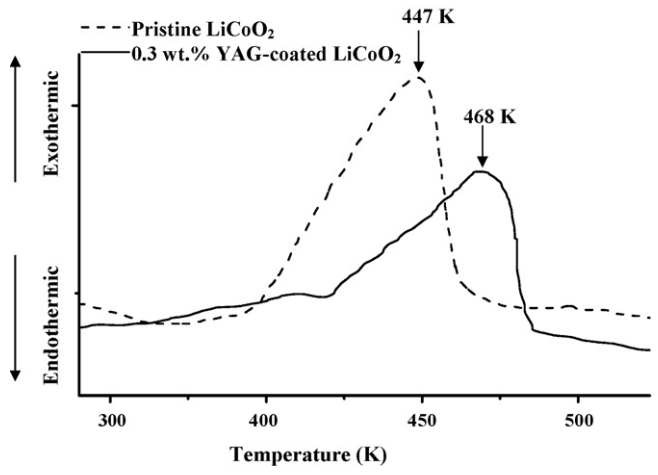

Fig. 15. DSC curves of the pristine and 0.3 wt.% YAG-coated $LiCoO_2$ cathode materials after fully charged at 4.4 V *vs.* Li for 20 h.

3.6. Thermal stability of the charged cathodes

Fig. 15 shows the DSC curves for pristine and 0.3 wt.% YAG-coated $LiCoO_2$ cathode materials. In Fig. 15, the pristine cathode material displays a characteristic exothermic peak with a thermal decomposition temperature at 447 K and reaction enthalpy of 44.5 J g^{-1}, whereas, the YAG-coated sample exhibited an exothermic peak centered at 468 K and lower reaction enthalpy of 21.55 J g^{-1}. The YAG coated sample increased the thermal decomposition temperature and stability of the charged coated cathode material by 21 K in the electrolyte compared to the pristine $LiCoO_2$ cathode, and this is attributed to the ability of YAG ceramic material to withstand high temperatures. In the process, the heat evolution is due to the decomposition and destruction of the layered structure with the release of oxygen, because of the instability of the highly oxidized Co^{4+} ions in the lattice at a constantly charged state, at high temperatures. The decrease in heat evolution agrees with existing literature on the coated samples compared to the uncoated samples [37–41]. YAG-coated $LiCoO_2$ cathode materials exhibited considerably less exothermic activity and reduced heat generation at a highly delithiated state, and thereby possessed better thermal safety characteristics than pristine $LiCoO_2$ cathode materials.

4. Conclusions

Various wt.% YAG sols were successfully coated on the surface of $LiCoO_2$ cathode materials by an in situ sol–gel method. XRD patterns showed a completely nanocrystalline YAG formed at 923 K and the YAG-coated materials did not show any secondary phase peaks or change in lattice parameters, which confirmed that the coating oxide remained on the surface. The TEM images confirmed that the nanocrystalline YAG particles, ranging from 90 to 120 nm in size, formed a compact coating over the cathode particle by an in situ sol–gel process, followed by heating at 923 K. Galvanostatic cycling studies showed an improvement in the cycle stability of 0.3 wt.% YAG-coated $LiCoO_2$, which is almost 7 times more stable than the 24 cycles sustained by the pristine cathode. The differential capacity plots of the coated cathode suggest that the YAG-coating protected the surface from faster impedance growth during electrochemical cycling and resulted in better cycle stability.

Acknowledgement

Financial support for this work was provided by the National Science Council of the Republic of China under contract no. NSC 93-2214-E-008-004.

References

[1] L.D. Dyer, B.S. Borie Jr., G.P. Smith, J. Am. Chem. Soc. 76 (1954) 1499.
[2] C. Delmas, M. Menetrier, L. Croguennec, I. Saadoune, A. Rougier, C. Pouillerie, G. Prado, M. Grune, L. Fournes, Electrochim. Acta 45 (1999) 243.
[3] J.M. Tarascon, M. Armand, Nature (London) 414 (2001) 359.
[4] C. Julien, S. Gastro-Garcia, J. Power Sources 97–98 (2001) 290.
[5] M. Winter, J.O. Besenhard, M.E. Spahr, P. Novák, Adv. Mater. 10 (1998) 725.
[6] J. Cho, G. Kim, Electrochem. Solid-State Lett. 2 (6) (1999) 253.
[7] Z. Chen, J.R. Dahn, Electrochem. Solid-State Lett. 5 (10) (2002) A213.
[8] Z. Chen, J.R. Dahn, Electrochim. Acta 49 (2004) 1079.
[9] Y. Jang, B. Haung, D.R. Sadoway, G. Ceder, Y.M. Chiang, H. Liu, H. Tamura, J. Electrochem. Soc. 146 (1999) 862.
[10] H. Tukamoto, A.R. West, J. Electrochem. Soc. 144 (1997) 3164.
[11] A.M. Kannan, L. Rabenberg, A. Manthiram, Electrochem. Solid-State Lett. 6 (2003) A16.
[12] J. Cho, Y.J. Kim, T.-J. Kim, B. Park, Angew. Chem. Int. Ed. 40 (2001) 3367.
[13] G.T.K. Fey, J.G. Chen, T.P. Kumar, J. Appl. Electrochem. 35 (2005) 177.
[14] G.T.K. Fey, J.G. Chen, T.P. Kumar, J. Power Sources 146 (2005) 250.
[15] G.T.K. Fey, P. Muralidharan, C.Z. Lu, Y.D. Cho, Solid State Ionics 177 (2006) 877.
[16] G.T.K. Fey, P. Muralidharan, Y.D. Cho, J. Power Sources 160 (2006) 1294.

[17] G.T.K. Fey, C.Z. Lu, T.P. Kumar, P. Muralidharan, A.S.T. Chiang, J. Phys. Chem. Solids 67 (2006) 2337.
[18] G.T.K. Fey, C.Z. Lu, T.P. Kumar, Y.C. Chang, Surf. Coat. Technol. 199 (2005) 22.
[19] G.T.K. Fey, H.Z. Yang, T.P. Kumar, S.P. Naik, A.S.T. Chiang, D.C. Lee, J.R. Lin, J. Power Sources 132 (2004) 172.
[20] G.T.K. Fey, Y.Y. Lin, T. Prem Kumar, Surf. Coat. Technol. 191 (2005) 68.
[21] G.T.K. Fey, P. Muralidharan, C.Z. Lu, Y.D. Cho, Electrochim. Acta 51 (2006) 4850.
[22] R.C. Pullar, M.D. Taylor, A.K. Bhattacharya, J. Eur. Ceram. Soc. 19 (1999) 1747.
[23] R.C. Pullar, A.K. Bhattacharya, Mater. Lett. 39 (1999) 173.
[24] M. Veith, S. Mathur, A. Kareiva, M. Jilavi, M. Zimmer, V. Huch, J. Mater. Chem. 9 (1999) 3069.
[25] Joint Commission on Powder Diffraction Standards (JCPDS) card No. 88-2047, International Center for Diffraction Data, PCPDFWIN version 2.3, 2002.
[26] J.R. Dahn, U. von Sacken, C.A. Michel, Solid State Ionics 44 (1990) 87.
[27] J.N. Reimers, E. Rossen, C.D. Jones, J.R. Dahn, Solid State Ionics 61 (1993) 335.
[28] G.G. Amatucci, J.M. Tarascon, L.C. Klein, Solid State Ionics 83 (1996) 167.
[29] D. Aurbach, B. Markovsky, A. Rodkin, E. Levi, Y.S. Cohen, H.J. Kim, M. Schmidt, Electrochim. Acta 47 (2002) 4291.
[30] K. Edstrom, T. Gustafsson, J.O. Thomas, Electrochim. Acta 50 (2004) 395.
[31] F. Croce, F. Nobili, A. Deptula, W. Lada, R. Tossici, A. D'Epifanio, B. Scrosati, R. Marassi, Electrochem. Commun. 1 (1999) 605.
[32] F. Nobili, F. Croce, B. Scrosati, R. Marassi, Chem. Mater. 13 (2001) 1642.
[33] D. Aurbach, A. Schechter, Electrochim. Acta 46 (2001) 2395.
[34] D. Aurbach, M.D. Levi, E. Levi, H. Teller, B. Markovsky, G. Salitra, L. Heider, U. Heider, J. Electrochem. Soc. 145 (1998) 3024.
[35] D. Aurbach, B. Markovsky, M.D. Levi, E. Levi, A. Schechter, M. Moshkovich, Y.S. Cohen, J. Power Sources 81–82 (1999) 95.
[36] D. Aurbach, B. Markovsky, A. Rodkin, M. Cojocaru, E. Levi, H.J. Kim, Electrochim. Acta 47 (2002) 1899.
[37] D.D. MacNeil, J.R. Dahn, J. Electrochem. Soc. 148 (2001) A1205.
[38] D.D. MacNeil, Zhonghua Lu, Zhaohui Chen, J.R. Dahn, J. Power Sources 108 (2002) 8.
[39] Y. Baba, S. Okada, J.-ichi. Yamaki, Solid State Ionics 148 (2002) 311.
[40] J. Cho, Electrochem. Commun. 5 (2003) 146.
[41] J. Cho, T.-G. Kim, C. Kim, J.-G. Lee, Y.-W. Kim, B. Park, J. Power Sources 146 (2005) 58.